Available online at www.sciencedirect.com
SCIENCE DIRECT®
International Journal of Solids and Structures 43 (2006) 3044–3056
INTERNATIONAL JOURNAL OF SOLIDS and STRUCTURES
www.elsevier.com/locate/ijsolstr

Observation and modeling of the anisotropic visco-hyperelastic behavior of a rubberlike material

Julie Diani [a,*], Mathias Brieu [b], Pierre Gilormini [a]

[a] Laboratoire d'Ingénierie des Matériaux, CNRS UMR 8006, ENSAM, 151 Bd de l'Hôpital, 75013 Paris, France
[b] Laboratoire de Mécanique de Lille, CNRS UMR 8107, Ecole Centrale de Lille, BP 48, 59651 Villeneuve d'Ascq, France

Received 4 February 2005; received in revised form 16 June 2005
Available online 15 August 2005

Abstract

The visco-hyperelastic behavior of a filled rubberlike material has been studied experimentally by large deformation cyclic uniaxial loadings, and an anisotropy induced by the Mullins effect has been demonstrated. By applying a generalized Maxwell model to a set of material directions, damage could be included in order to reproduce the stress softening due to the Mullins effect. This induces also an anisotropic mechanical response, and the model compares favorably with the experimental measures.

Keywords: Constitutive model; Visco-hyperelasticity; Anisotropy; Finite deformation; Mullins effect; Rubber

1. Introduction

Despite a large number of publications in the last decade, the accurate prediction of the mechanical behavior of rubberlike materials remains an open issue (Dorfmann and Ogden, 2004). These materials are often used under cyclic conditions, where large deformation viscoelasticity coupled with damage is relevant. Their mechanical behavior has been described first as hyperelastic, and several forms of strain energy density have been defined so far, see for instance Rivlin and Saunders (1951), Hart-Smith (1966), Ogden (1972), Lambert-Diani and Rey (1999) and Boyce and Arruda (2000). Later, the stress softening induced by the first loading cycle, and known as the Mullins effect (Mullins and Tobin, 1947), has been included in constitutive equations by adding damage. An isotropic damage parameter D has often been introduced

* Corresponding author. Fax: +33 1 44 24 62 90.
E-mail address: julie.diani@paris.ensam.fr (J. Diani).

0020-7683/$ - see front matter © 2005 Elsevier Ltd. All rights reserved.
doi:10.1016/j.ijsolstr.2005.06.045

in order to modify the strain energy density by the multiplicative factor $1 - D$ (Simo, 1987; Govindjee and Simo, 1991; Miehe, 1995; Ogden and Roxburgh, 1999; Beatty and Krishnaswamy, 2000). In an alternative approach based on macromolecular models, still assuming isotropy, Marckmann et al. (2002) have proposed to account for damage by making the average length and volume fraction of the chains that support stress depend on the loading history.

Early experimental results (Mullins, 1948; Harwood and Payne, 1966; Mullins, 1969) have demonstrated the viscoelastic character of rubberlike materials. For instance, the uploading and unloading responses differ during cyclic loadings. Many visco-hyperelastic constitutive models with or without damage have been proposed by Simo (1987), Lion (1998), Reese and Govindjee (1998), Bergström and Boyce (1998), Miehe and Keck (2000), Huber and Tsakmakis (2000), Kaliske et al. (2001), Reese (2003) and Laiarinandrasana et al. (2003), among others. In these papers, the material is always considered as isotropic, although it has been reported for long that some anisotropy is induced by the Mullins effect (Mullins, 1948). This has been taken into account in the limited context of hyperelasticity or viscoelasticity, by using suitable tensorial representations (Holzapfel and Gasser, 2001; Horgan et al., 2004) or by combining damage and a model based on a set of material directions (Pawelski, 2001). This has been applied to describe the initial anisotropy, as may be found in calendered plates for instance, by Itskov and Aksel (2004), who used the tensorial approach, or by Diani et al. (2004), who used a set of material directions.

In this work, cyclic uniaxial tension tests have been performed in order to analyze the viscoelastic behavior of a rubberlike material, with emphasis put on the anisotropy induced by the Mullins effect, as reported in Section 2. Section 3 shows how the mechanical response of the material can be represented by combining a generalized Maxwell scheme and a model using a set of damageable material directions. Here, damage refers to the Mullins strain-induced stress softening and is introduced as an anisotropic extension of the network alteration theory of Marckmann et al. (2002). Each material direction undergoes a softening that depends on the largest stretch that it has ever been submitted to. This model is shown to be in agreement with the second law of thermodynamics and is able to represent visco-hyperelasticity with stress softening as well as initial and induced anisotropies. It is favorably compared with experimental data in Section 4.

2. Experimental observations

All the tests presented here were conducted on an Instron 4302 uniaxial testing machine operated in the local strain control mode, where local strains were measured by video image analysis, at a low and constant strain rate of $0.01\ s^{-1}$. The material was a commercial EPDM (ethylene propylene diene) elastomer filled with carbon black and processed in plates of 2 mm thickness. The specimens were 10 mm long and 4 mm wide, except in some cases that are explicitly specified in the text.

Fig. 1a shows the stress–strain response obtained under cyclic loading conditions. During this test, the maximum strain is increased after each 10-cycle series. The material response at the first cycle of each series differs significantly from the responses at the next cycles. This large difference is due to the Mullins effect, which is a strain-induced stress softening phenomenon that has been extensively studied by Mullins and coworkers (Mullins and Tobin, 1947; Mullins, 1948; Mullins, 1969). After the second cycle, the material softens gradually by fatigue. This effect has been shown to be non-negligible (Gentot et al., 2004) but, since the present work focuses on the Mullins effect, it will not be studied here, and each series of cycles will be limited to a single loading–unloading–reloading sequence (Fig. 1b). A method for including fatigue softening in the model will be suggested in Section 3.2. In order to evaluate the elastic part from the overall viscoelastic response, a test has been performed, where loading periods and stress-relaxation periods were applied sequentially. It can be observed in Fig. 1c that the material response tends towards an equilibrium state, which cannot be reached within laboratory time scale and is closer to the unloading curve than to the loading curve.

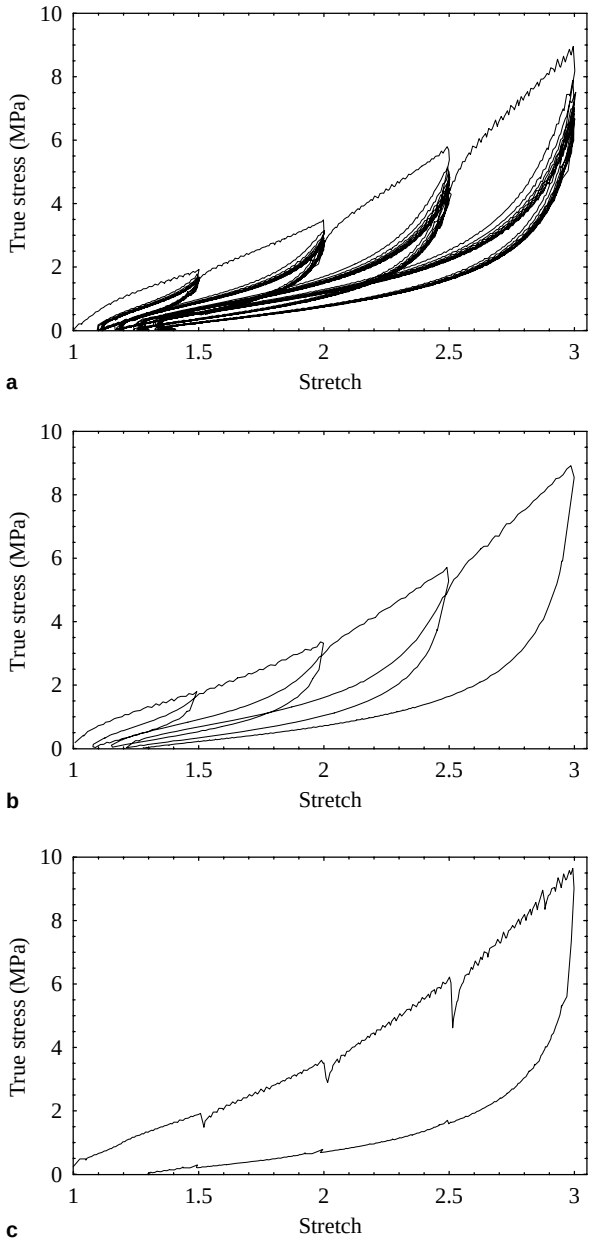

Fig. 1. Stress–strain behavior of a carbon black filled EPDM elastomer in uniaxial tension. (a) Ten cycles applied at 50%, 100%, 150%, and 200% stretch. (b) Load–unload–reload sequences applied at the same stretch levels. (c) Stress relaxation applied at the same stretch levels, during loading and unloading.

The initial in-plane isotropy of the material has been checked by conducting uniaxial tension tests on specimens that were cut from the plate with various orientations, which lead to indistinguishable responses. In order to study the anisotropy induced by the Mullins effect, two identical large specimens (60 mm long and 25 mm wide) were submitted to two cycles of 200% stretch in uniaxial tension along a direction referred

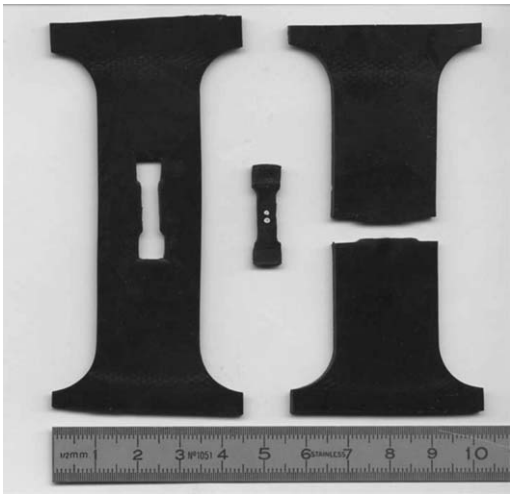

Fig. 2. The large and small samples used. The white painted dots are used by the video extensometer.

to as 'direction 1'. Then, a smaller specimen was cut from each of these preconditioned large samples, either along direction 1 (sample 1) or along the orthogonal direction (sample 2), as illustrated in Fig. 2. Samples 1 and 2 were subsequently submitted to two cycles of 200% uniaxial tension. As a consequence, both small samples had the same preconditioning, where the Mullins effect lead to the same stress softening, but they were loaded along different material directions, which allows for checking if some anisotropy has been induced by the preconditioning. One would expect a response of sample 1 (loaded the same way as in preconditioning) similar to what had been observed on the large samples, and sample 2 (loaded perpendicularily to preconditioning) may behave differently, depending on the magnitude of the anisotropy.

The stress vs. stretch (using a reference length measured on the virgin material) responses obtained with the large sample and with the two small samples are shown in Fig. 3. Sample 1 shows a curve shape that is similar to the one observed on the large sample at the second cycle. This shape is typical of a material where

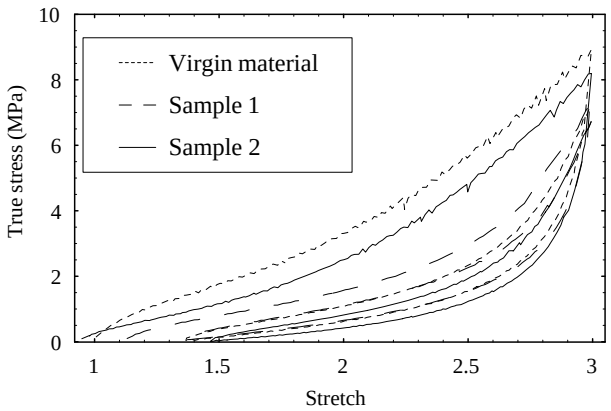

Fig. 3. Anisotropy induced by the Mullins effect: uniaxial stress–strain responses (load–unload–reload) of a carbon black filled EPDM elastomer preliminarily submitted to a uniaxial tension (two cycles) along direction 1 and subsequently loaded either along direction 1 or along the perpendicular direction 2.

the Mullins effect has been already saturated. The beginning of the curve for sample 1 differs from the second cycle of the large specimen: it starts at a lower stretch and requires one cycle to reach the curve of the large sample. This is due to some relaxation of the viscoelastic strains: after unloading the large sample, there remains a stretch of about 31%, which is partially recovered during the 20 min that are required to cut and prepare the small sample. When the latter is ready for testing, a residual stretch of 13% is measured. It has been checked also that this residual stretch was still 12% after 48 h, which shows the viscous nature of a part of the strain that remains after instantaneous elastic unloading of the material, most of which is recovered after 20 min. The curve for sample 2 starts from a residual contraction, which is consistent with the residual elongation in direction 1 and with the incompressibility of the material. During the first load, sample 2 exhibits a shape curve that is similar to the one observed on the large sample at the first load, which suggests that the Mullins effect is not saturated yet. Some softening has already been endured by the material, though, since the first loading of sample 2 is below the response of the large sample. During the second cycle of sample 2, no more Mullins effect is observed and the curve is similar to the second cycles of the large sample and of sample 1, with some shift towards higher stretches. Samples 1 and 2 clearly show different responses which illustrate the anisotropy induced by the Mullins effect.

3. Anisotropic visco-hyperelastic model including damage

3.1. General theory of incompressible visco-hyperelastic materials

The generalized Maxwell model that is shown in Fig. 4 is likely to represent the behavior of elastomers correctly, since it tends gradually to an equilibrium elastic state (Fig. 1c) during a long relaxation test, for instance. It is similar to other models that have been used previously to define isotropic visco-hyperelastic constitutive equations for filled rubberlike materials (Holzapfel and Simo, 1996; Bergström and Boyce, 1998; Miehe and Keck, 2000; Kaliske et al., 2001; Reese, 2003), but here the responses of the hyperelastic springs evolve with damage and include anisotropy in the three-dimensional generalization of the model. The constitutive equations based on this rheological model are built in three steps. First, the general theory of an incompressible visco-hyperelastic material is rapidly described. Then, the various components of the

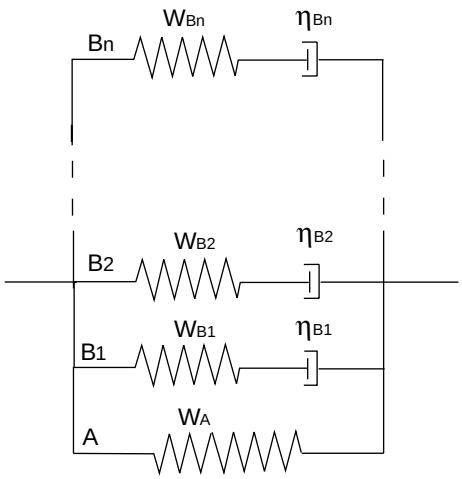

Fig. 4. The rheological model used. The springs are hyperelastic, and they are anisotropic and damageable in the three-dimensional generalization.

model are defined by using a set of material directions which allows for a globally anisotropic response. Finally, a damage variable is introduced for each material direction in order to reproduce the stress softening associated with the Mullins effect.

The general theory of viscoelasticity at finite strains has been detailed very precisely by Reese and Govindjee (1998), and it suffices to recall here the main equations. For instance, it is essential that the second law of thermodynamics be satisfied, which leads to

$$\tfrac{1}{2}\mathbf{S} : \dot{\mathbf{C}} - \dot{\mathscr{W}} \geqslant 0, \tag{1}$$

where $\mathbf{S}$ denotes the second Piola–Kirchhoff stress, $\mathbf{C}$ is the right Cauchy–Green tensor, and $\mathscr{W}$ is the total free energy. In the rheological model of Fig. 4, $\mathscr{W}$ is given by

$$\mathscr{W} = \mathscr{W}_A(\mathbf{C}) + \sum_{k=1,n} \mathscr{W}_{B_k}(\mathbf{C}_e^{B_k}), \tag{2}$$

where $\mathscr{W}_A$ denotes the strain energy of the material at equilibrium state, and $\mathscr{W}_{B_k}$ is the strain energy of the spring in branch B_k. As suggested by Sidoroff (1974), for instance, the total deformation gradient can be decomposed as follows in branch B_k:

$$\mathbf{F}^{B_k} = \mathbf{F}_e^{B_k} \cdot \mathbf{F}_v^{B_k}, \tag{3}$$

where $\mathbf{F}_e^{B_k}$ and $\mathbf{F}_v^{B_k}$ are the deformation gradients associated with the spring and the dashpot, respectively. Therefore, $\mathbf{C}_e^{B_k} = (\mathbf{F}_e^{B_k})^{\mathrm{T}} \cdot \mathbf{F}_e^{B_k}$ is the elastic right Cauchy–Green tensor in branch B_k. By substitution of (2) in (1), and after some derivations detailed in Reese and Govindjee (1998), one gets

$$\mathbf{S} = 2\frac{\partial \mathscr{W}_A}{\partial \mathbf{C}} + 2\sum_{k=1,n} (\mathbf{F}_v^{B_k})^{-1} \cdot \frac{\partial \mathscr{W}_{B_k}}{\partial \mathbf{C}_e^{B_k}} \cdot (\mathbf{F}_v^{B_k})^{-\mathrm{T}} \quad \text{and} \quad \sum_{k=1,n} \frac{\partial \mathscr{W}_{B_k}}{\partial \mathbf{C}_e^{B_k}} : \left(\mathbf{C}_e^{B_k} \cdot \mathbf{L}_v^{B_k}\right) \geqslant 0. \tag{4}$$

The elastic part of the material response is given by $\mathbf{S}_e = 2\frac{\partial \mathscr{W}_A}{\partial \mathbf{C}}$, the viscous part is $\mathbf{S}_v = \mathbf{S} - \mathbf{S}_e$, and $\mathbf{L}_v^{B_k} = \dot{\mathbf{F}}_v^{B_k} \cdot (\mathbf{F}_v^{B_k})^{-1}$ is the velocity gradient associated with the viscous part of the deformation gradient in branch B_k.

Rubberlike materials are quasi-incompressible, and strict incompressibility is usually assumed when dealing with loading conditions such as uniaxial tension, pure shear or equibiaxial tension. Therefore, the material will be considered as incompressible in the present work and, more specifically, incompressibility is assumed to apply to both the elastic and viscous components:

$$\det\left(\mathbf{F}^A\right) = \det(\mathbf{F}) = 1 \quad \text{and} \quad \det\left(\mathbf{F}_e^{B_k}\right) = \det\left(\mathbf{F}_v^{B_k}\right) = 1 \quad \forall k. \tag{5}$$

Hence, relations (4) become (Le Tallec et al., 1993):

$$\mathbf{S} = 2\frac{\partial \mathscr{W}_A}{\partial \mathbf{C}} + 2\sum_{k=1,n} (\mathbf{F}_v^{B_k})^{-1} \cdot \frac{\partial \mathscr{W}_{B_k}}{\partial \mathbf{C}_e^{B_k}} \cdot (\mathbf{F}_v^{B_k})^{-\mathrm{T}} - p\mathbf{C}^{-1} \quad \text{and}$$
$$\sum_{k=1,n} \left(\frac{\partial \mathscr{W}_{B_k}}{\partial \mathbf{C}_e^{B_k}} - q^{B_k} \left(\mathbf{C}_e^{B_k}\right)^{-1} \right) : \left(\mathbf{C}_e^{B_k} \cdot \mathbf{L}_v^{B_k}\right) \geqslant 0, \tag{6}$$

where p and q^{B_k} are Lagrange multipliers. In order to get stresses, one needs to define the elastic deformation gradient $\mathbf{F}_e^{B_k}$ in each branch B_k in such a way that the inequality in (6) is satisfied. A sufficient condition (among other possibilities) for this requirement is obtained by prescribing

$$\mathbf{L}_v^{B_k} = \frac{1}{\eta^{B_k}} \left(\mathbf{C}_e^{B_k} \cdot \frac{\partial \mathscr{W}_{B_k}}{\partial \mathbf{C}_e^{B_k}} - q^{B_k}\mathbf{I} \right) \quad \forall k, \tag{7}$$

where $\mathbf{I}$ denotes the identity tensor, and where the viscosity $\eta^{B_k} > 0$ has been introduced to characterize the dashpot in branch B_k. Since, according to (3), the velocity gradient $\mathbf{L}$ is related to $\mathbf{L}_v^{B_k}$ and $\mathbf{L}_e^{B_k}$ by

$$\mathbf{L} = \mathbf{L}_{\mathrm{e}}^{B_k} + \mathbf{F}_{\mathrm{e}}^{B_k} \cdot \mathbf{L}_{\mathrm{v}}^{B_k} \cdot (\mathbf{F}_{\mathrm{e}}^{B_k})^{-1}, \tag{8}$$

the equation of evolution takes the following form:

$$\mathbf{L} = \mathbf{L}_{\mathrm{e}}^{B_k} + \frac{1}{\eta^{B_k}} \mathbf{F}_{\mathrm{e}}^{B_k} \cdot \left(\mathbf{C}_{\mathrm{e}}^{B_k} \cdot \frac{\partial \mathscr{W}_{B_k}}{\partial \mathbf{C}_{\mathrm{e}}^{B_k}} - q^{B_k} \mathbf{I} \right) \cdot (\mathbf{F}_{\mathrm{e}}^{B_k})^{-1} \quad \forall k. \tag{9}$$

It should be noted that Eqs. (6) and (9) do not restrict to isotropic behaviors, and this general theory is applied below to an anisotropic set of material directions. Moreover, damage can be included easily as a series of parameters D_i $(i = 1, \ldots, 1)$, if the condition

$$-\frac{\partial \mathscr{W}}{\partial D_i} \dot{D}_i \geqslant 0 \tag{10}$$

applies for all i, since this ensures that the Clausius–Duhem inequality is still satisfied.

3.2. Application to a model based on damageable material directions

Hyperelastic laws for rubberlike materials based on sets of material directions have been proposed previously by Pawelski (2001) and Diani et al. (2004). In such models, which are able to account for anisotropy, the hyperelastic strain energy density is approximated by summing contributions over a set of material directions. A unit vector parallel to one of the m directions considered is denoted $\mathbf{u}^i$; it is defined on the reference configuration, i.e., it does not vary when the material deforms. If a deformation gradient $\mathbf{F}$ is applied, each direction is stretched with

$$\lambda^i = \sqrt{(\mathbf{F}\mathbf{u}^i)^{\mathrm{T}} \cdot (\mathbf{F}\mathbf{u}^i)} = \sqrt{\mathbf{u}^i \cdot \mathbf{C} \cdot \mathbf{u}^i}. \tag{11}$$

The total strain energy of the system is thus given by

$$\mathscr{W} = \sum_i n^i w(\lambda^i, N^i), \tag{12}$$

where n^i is the volume fraction of molecular chains whose end-to-end vectors are parallel to $\mathbf{u}^i$, and w is an elementary strain energy:

$$w(\lambda^i, N^i) = N^i bT \left[\beta \frac{\lambda^i}{\sqrt{N^i}} + \ln\left(\frac{\beta}{\sinh \beta} \right) \right] \quad \text{with } \beta = \mathscr{L}^{-1}\left(\frac{\lambda^i}{\sqrt{N^i}} \right), \tag{13}$$

denoting $\mathscr{L}^{-1}$ the inverse of the Langevin function. Actually, (13) is the elementary density of a non-Gaussian macromolecular chain (Treloar, 1975), b denotes Boltzmann's constant, and T is the absolute temperature. Parameter N^i relates to the maximum possible extension along direction $\mathbf{u}^i$ and equals the number of links in a chain in the classical macromolecular context.

The strain energy densities $\mathscr{W}_A$ and $\mathscr{W}_{B_k}$ of the previous section are now defined by using (12):

$$\begin{aligned} \mathscr{W}_A(G^{iA}, N^{iA}, \mathbf{C}) &= \sum_i n^{iA} w(\lambda^{iA}, N^{iA}), \quad \lambda^{iA} = \sqrt{\mathbf{u}^i \cdot \mathbf{C} \cdot \mathbf{u}^i}, \\ \mathscr{W}_{B_k}(G^{iB_k}, N^{iB_k}, \mathbf{C}_{\mathrm{e}}^{B_k}) &= \sum_i n^{iB_k} w(\lambda_{\mathrm{e}}^{iB_k}, N^{iB_k}), \quad \lambda_{\mathrm{e}}^{iB_k} = \sqrt{\mathbf{u}^i \cdot \mathbf{C}_{\mathrm{e}}^{B_k} \cdot \mathbf{u}^i}, \end{aligned} \tag{14}$$

where the parameters $G^{iA} = n^{iA} bTN^{iA}$ and $G^{iB_k} = n^{iB_k} bTN^{iB_k}$ have been introduced. Eqs. (13), (14), (6) and (9) define a material that may be anisotropic, depending on the values of the parameters G^{iA}, G^{iB_k}, N^{iA} and N^{iB_k}. Since it has been demonstrated in Section 2 that the loading history induces some anisotropy in an initially isotropic material, a damage variable is now introduced along each direction, that will act on all these parameters.

In order to account for the strain-induced stress softening due to the Mullins effect, Marckmann et al. (2002) have proposed to include damage in macromolecular models as an increase of the average chain length with the average chain stretch. This model has been defined initially on the isotropic eight-chain model of Arruda and Boyce (1993) and applied later to the isotropic full-network model by Diani and Gilormini (in press). The physical interpretations of damage in the macromolecular network that are detailed in Marckmann et al. (2002) suggest that the number of active chain links is constant, and therefore the number of chains under stress decreases if the average chain length increases. This assumption is extended here to all the material directions considered, and to all the hyperelastic components of the rheological model:

$$n^{iA}(t)N^{iA}(t) = \text{cst} \quad \text{and} \quad n^{iB_k}(t)N^{iB_k}(t) = \text{cst} \quad \forall k, \ \forall i, \ \forall t. \tag{15}$$

For each direction $\mathbf{u}^i$, the parameters N^{iA} and N^{iB_k} are assumed to depend on the largest elastic stretch values $\lambda^{iA}_{\max}$ and $\lambda^{iB_k}_{\max}$ ever reached along this direction. Since no quantitative experimental observation of the mean chain length before and after damage is available, an empirical form is proposed for this dependence:

$$N^{iA}/N^{iA}_0 = \alpha(\lambda^{iA}_{\max} - 1)^2 + 1 \quad \text{with } \lambda^{iA}_{\max}(t) = \max_{\tau\in[0,t]} \lambda^{iA}(\tau), \tag{16}$$

where N^{iA}_0 is the initial value of N^{iA}, and $\alpha > 0$ is a material damage parameter, with similar equations for N^{iB_k}. This damage evolution law is proposed to fit the experimental data obtained on the elastomer considered in the present study, and it may be inadequate for other materials. It depends probably on the nature, shape and amount of filler particles, in addition to the nature of the gum and the vulcanization process, but this question is beyond the scope of this paper. While N^{iA} and N^{iB_k} increase with $\lambda^{iA}_{\max}$ and $\lambda^{iB_k}_{\max}$, respectively, the fractions of active chains n^{iA} and n^{iB_k} decrease because of (15), but G^{iA} and G^{iB_k} remain constant. Since $\lambda^{iA}_{\max}$ and $\lambda^{iB_k}_{\max}$ depend on $\mathbf{u}^i$, this provides an easy way of generating an anisotropic response of the material, as compared to the tensorial approaches of Holzapfel and Gasser (2001) and of Horgan et al. (2004), which are limited to specific anisotropies.

The introduction of the Mullins effect into the constitutive equations can now be performed by adding $\lambda^{iA}_{\max}$ and $\lambda^{iB_k}_{\max}$ as internal variables that will modify N^{iA} and N^{iB_k}:

$$\mathscr{W}(\mathbf{C}, \mathbf{C}^{B_k}_{\mathrm{e}}, \lambda^{iA}_{\max}, \lambda^{iB_k}_{\max}) \quad \text{with } i \in \{1,\dots,m\} \text{ and } k \in \{1,\dots,n\}. \tag{17}$$

There remains to verify that (10) is satisfied, where D_i is replaced by $\lambda^{iA}_{\max}$ or $\lambda^{iB_k}_{\max}$. First, the evolution law (16) ensures that $\dot{\lambda}^{iA}_{\max} \geqslant 0$, $\dot{\lambda}^{iB_k}_{\max} \geqslant 0$, $\frac{\partial N^{iA}}{\partial \lambda^{iA}_{\max}} \geqslant 0$, and $\frac{\partial N^{iB_k}}{\partial \lambda^{iB_k}_{\max}} \geqslant 0$. Moreover, the definition of $\mathscr{W}$ given in (12) gives

$$\frac{\partial \mathscr{W}}{\partial N^{iA}} = -\frac{\lambda^{iA} G^{iA}}{2N^{iA}\sqrt{N^{iA}}} \mathscr{L}^{-1}\left(\frac{\lambda^{iA}}{\sqrt{N^{iA}}}\right), \tag{18}$$

with similar expressions for the B_k components. An elementary study of the inverse Langevin function shows that $\frac{\partial \mathscr{W}}{\partial N^{iA}} \leqslant 0$ and $\frac{\partial \mathscr{W}}{\partial N^{iB_k}} \leqslant 0$ as long as $\lambda^{iA} \leqslant \sqrt{N^{iA}}$ and $\lambda^{iB_k}_{\mathrm{e}} \leqslant \sqrt{N^{iB_k}}$, and consequently the Clausius–Duhem inequality is satisfied.

It may be noted that N^i changes because of the Mullins effect only in the above theory, but fatigue may also be accounted for by making N^i depend on some measure of the stretch history rather than merely on the maximum stretch ever reached. If the material is isotropic initially, the number of initial parameters is reduced since $N^{iA}_0 = N^A_0$, $N^{iB_k}_0 = N^{B_k}_0$, $G^{iA}_0 = G^A_0$ and $G^{iB_k}_0 = G^{B_k}_0$ for all directions $\mathbf{u}^i$. The latter should be distributed as regularly as possible in order to account for isotropy, and the 16 directions defined by the 32 vertices (each vertex has an opposite) of the polyhedron shown in Fig. 5 are used, like in Pawelski (2001). This polyhedron is obtained from a dodecahedron where an additional vertex has been added in the direction of the center of each of the 12 pentagonal faces. Thus, each pentagonal face leads to five triangular faces, and one finally gets 12 vertices where five edges join, and 20 vertices where six edges join. As

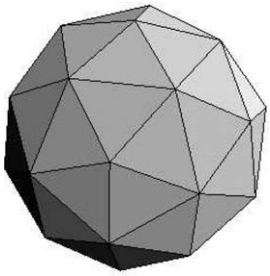

Fig. 5. Thirty two-vertex polyhedron where the 16 directions used are defined: six directions joining opposite five-edge vertices, and 10 directions joining opposite six-edge vertices.

mentioned in Bažant and Oh (1986), an average over these directions should use weights of $\frac{25}{420}$ and $\frac{27}{420}$ for the six directions joining two opposite five-edge vertices and for the 10 directions joining two opposite six-edge vertices, respectively. For checking how well isotropy is satisfied with this set of directions, uniaxial tension tests and pure shear tests were simulated with randomly chosen orientations, which lead to a discrepancy below 5%. This precision is considered as sufficient in the present work, but a better approximation of isotropy can be obtained by using more directions, if necessary. For instance, subdividing each face of the above polyhedron into four smaller triangles leads to a total of 61 directions, whose weights are also given by Bažant and Oh (1986).

4. Comparison with the experimental data

A large number of viscoelastic branches is likely to be necessary to fit the stress–time curve of a relaxation test precisely but, for the sake of simplicity, we will restrict the number of viscoelastic branches to two. The first one is related to mechanisms inducing short-time relaxation, and the other one defines long-time relaxation. The long-time relaxation branch will allow to account for a viscous stress that increases with the maximum stretch reached, as can be observed in Fig. 1c, while the short-time relaxation will provide the hysteresis observed during a loading–unloading cycle (Fig. 1b). Hence, the general rheological model introduced in Fig. 4 is simplified with only two viscoelastic branches B_1 and B_2 in addition to the hyperelastic branch A. The response of this model is compared below to the experimental data of Section 2. First, the model parameters are fitted on the stress–strain response to a uniaxial cyclic loading (Fig. 1b). Then, the ability of the model to reproduce the Mullins induced anisotropy (Fig. 3) is tested.

Application of the model to uniaxial tension is detailed in Appendix A. The material parameters to be fitted are N_0^A, $N_0^{B_1}$, $N_0^{B_2}$, G^A, G^{B_1}, G^{B_2}, η^{B_1}, η^{B_2} and α. Our goal here is to catch the main features of the observed material behavior, and especially the anisotropy, with a minimum number of parameters. Hence, different α values are not considered for branches A, B_1 and B_2, and N_0^A, $N_0^{B_1}$ and $N_0^{B_2}$ are taken equal. The remaining seven parameters have been fitted simultaneously on the experimental stress–strain curves in Fig. 1b, leading to $\alpha = 0.4$, $N_0^A = N_0^{B_1} = N_0^{B_2} = 5$, $G^A = 0.6$ MPa, $G^{B_1} = 0.4$ MPa, $G^{B_2} = 2.0$ MPa, $\eta^{B_1} = 20.0$ MPa s^{-1}, and $\eta^{B_2} = 0.4$ MPa s^{-1}. The curves predicted by the model when using these values are shown in Fig. 6b and can be compared to the experimental measures repeated in Fig. 6a. The response of the model displays several typical features of the behavior of filled rubberlike materials: hysteresis, stress softening after the first cycle, and permanent set. During unloading, the stress decreases more gradually than in the experimental curve, where a large viscous stress that increases with the maximum stretch applied to the material (Fig. 1c) relaxes from the very beginning of unloading. A complete study of the stress–time relaxation behavior would be necessary to account for this characteristic correctly, which is beyond the

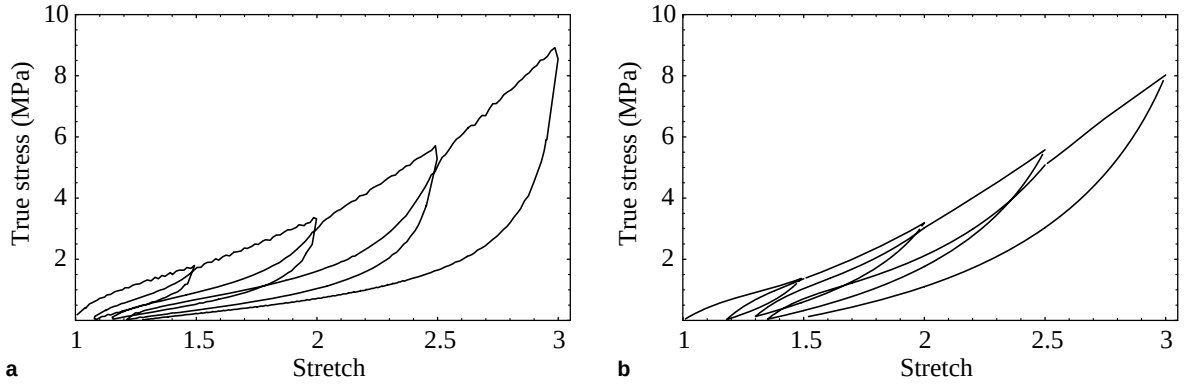

Fig. 6. Cyclic uniaxial tension: experimental data (a) and model prediction (b).

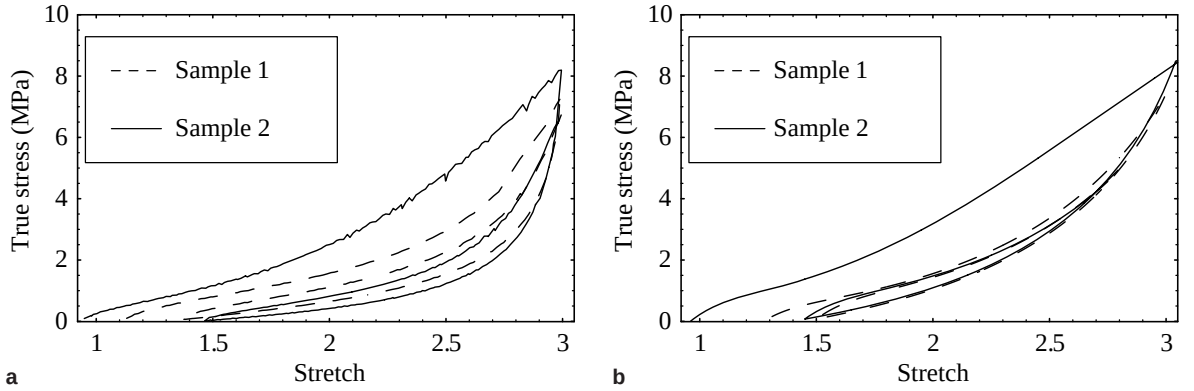

Fig. 7. Anisotropy induced by the Mullins effect: experimental data (a) and model prediction (b).

scope of this paper. It has been observed during the fitting procedure that increasing the value of η^{B_1} or η^{B_2} increases the viscous stress, but the relaxation time is increased as well, unfortunately. Finally, it has also been observed during the fitting procedure that the amount of permanent strain depends strongly on the damage parameter α.

Thus, the model reproduces reasonably well a non-linear stress–strain response, an hysteresis that is larger at the first cycle than at the second one, a strain-induced stress softening, and a permanent set. Comparison with the experimentally observed anisotropy (Fig. 7) shows that the model also catches a large difference between the two samples presented in Section 2. In agreement with the experimental data, sample 1 behaves like a material where the Mullins effect is saturated, while sample 2 still presents some Mullins effect at the first loading, as shown by a higher maximum stress and a large hysteresis at the first cycle. Like in Fig. 6, where the Mullins effect was not saturated, the stress decrease is too gradual for sample 2. It may also be noted that the shifts of the unloading and reloading curves of sample 1 are underestimated by the model.

5. Conclusion

Under cyclic loading conditions, filled rubberlike materials present a non-linear visco-hyperelastic behavior with damage. At the first cycle, the material undergoes a large strain-induced stress softening,

known as the Mullins effect, with a permanent strain and an induced anisotropy. An experimental procedure has been defined to measure the induced anisotropy. The latter has been demonstrated experimentally.

To reproduce these features, a visco-hyperelastic law based on a damageable generalized Maxwell model has been proposed. It has been shown to be in agreement with the requirements of thermodynamics, and it has been applied to a set of material directions that allows to account for initial and induced anisotropies easily, unlike other existing models.

The model compares favorably with the experiments. It is able to reproduce the main features of uniaxial cyclic stress–strain curves. In particular, a variation of the amount of hysteresis between the first and second cycles is obtained, as well as a Mullins strain-induced stress softening, and a permanent set. Moreover, the model reproduces the characteristics of the Mullins induced anisotropy that have been observed experimentally.

Acknowledgements

Support for this research was provided by the Manufacture Française de Pneumatiques Michelin and is acknowledged. The authors are grateful to Jean–Michel Vacherand for helpful discussions.

Appendix A

In this appendix, application of the model to uniaxial tension is detailed. A uniaxial tension is performed in direction $\mathbf{e}_1$ of a fixed reference frame $(\mathbf{e}_1, \mathbf{e}_2, \mathbf{e}_3)$, and is defined by the stretch history $\Lambda(t)$. Since the material is assumed isotropic initially, its response will be identical along directions $\mathbf{e}_2$ and $\mathbf{e}_3$. Therefore, using the assumed incompressibility (5), the only non-zero components of the deformation gradients are $F_{11} = \Lambda$, $F_{22} = F_{33} = 1/\sqrt{\Lambda}$, $(F_{\mathrm{v}}^{B_k})_{11} = \Lambda_{\mathrm{v}}^{B_k}$, $(F_{\mathrm{v}}^{B_k})_{22} = (F_{\mathrm{v}}^{B_k})_{33} = 1/\sqrt{\Lambda_{\mathrm{v}}^{B_k}}$, and $(F_{\mathrm{e}}^{B_k})_{11} = \Lambda_{\mathrm{e}}^{B_k}$, $(F_{\mathrm{e}}^{B_k})_{22} = (F_{\mathrm{e}}^{B_k})_{33} = 1/\sqrt{\Lambda_{\mathrm{e}}^{B_k}}$, with $\Lambda_{\mathrm{e}}^{B_k}\Lambda_{\mathrm{v}}^{B_k} = \Lambda$. The Cauchy stress $\boldsymbol{\sigma} = \frac{1}{\det \mathbf{F}}\mathbf{F}\cdot\mathbf{S}\cdot\mathbf{F}^{\mathrm{T}}$ can then be obtained from (6), and the non-zero component applied in the tensile test is given by

$$\sigma(\Lambda) = \sigma_{11} - \sigma_{22} = 2\Lambda^2\frac{\partial \mathscr{W}_A}{\partial C_{11}} + 2\sum_{k=1,n}(\Lambda_{\mathrm{e}}^{B_k})^2\frac{\partial \mathscr{W}_{B_k}}{\partial (C_{\mathrm{e}}^{B_k})_{11}} - 2\Lambda^{-1}\frac{\partial \mathscr{W}_A}{\partial C_{22}} - 2\sum_{k=1,n}(\Lambda_{\mathrm{e}}^{B_k})^{-1}\frac{\partial \mathscr{W}_{B_k}}{\partial (C_{\mathrm{e}}^{B_k})_{22}} \tag{A.1}$$

and, using the set of material directions $\mathbf{u}_i$ introduced in Section 3.2:

$$\sigma(\Lambda) = 2\sum_{i=1,m}\left[(\Lambda u_1^i)^2 - \frac{(u_2^i)^2}{\Lambda}\right]\frac{G^A}{\sqrt{N^A}}\mathscr{L}^{-1}\left(\frac{\lambda^i}{\sqrt{N^A}}\right) + 2\sum_{i=1,m}\sum_{k=1,n}\left[(\Lambda_{\mathrm{e}}^{B_k} u_1^i)^2 - \frac{(u_2^i)^2}{\Lambda_{\mathrm{e}}^{B_k}}\right]\frac{G^{B_k}}{\sqrt{N^{B_k}}}\mathscr{L}^{-1}\left(\frac{\lambda^{iB_k}}{\sqrt{N^{B_k}}}\right). \tag{A.2}$$

There remains to specify $\Lambda_{\mathrm{e}}^{B_k}$ in order to obtain $\sigma(\Lambda)$. This is done by rewriting the evolution law (9) as

$$\mathbf{L} = \mathbf{L}_{\mathrm{e}}^{B_k} + \frac{1}{\eta^{B_k}}\mathbf{B}_{\mathrm{e}}^{B_k}\cdot\boldsymbol{\sigma}^{B_k}\cdot(\mathbf{B}_{\mathrm{e}}^{B_k})^{-1}, \tag{A.3}$$

where the elastic left Cauchy–Green tensor $\mathbf{B}_{\mathrm{e}}^{B_k} = \mathbf{F}_{\mathrm{e}}^{B_k}\cdot(\mathbf{F}_{\mathrm{e}}^{B_k})^{\mathrm{T}}$ and the Cauchy stress $\boldsymbol{\sigma}^{B_k}$ in branch B_k have been introduced. For uniaxial tension, this tensorial relation simplifies into

$$\frac{\dot{\Lambda}}{\Lambda} = \frac{\dot{\Lambda}_{\mathrm{e}}^{B_k}}{\Lambda_{\mathrm{e}}^{B_k}} + \frac{1}{\eta^{B_k}}\sigma^{B_k} \quad \forall k \tag{A.4}$$

and leads to

$$\Lambda_{\mathrm{e}}^{B_k}(t) = \Lambda(t)\exp\left(-\frac{1}{\eta^{B_k}}\int_0^t \sigma^{B_k}\,\mathrm{d}\tau\right) \quad \forall k, \tag{A.5}$$

where σ^{B_k} is given by

$$\sigma^{B_k} = \sum_{i=1,m}\left[(\Lambda_{\mathrm{e}}^{B_k}u_1^i)^2 - \frac{(u_2^i)^2}{\Lambda_{\mathrm{e}}^{B_k}}\right]\frac{G^{B_k}}{\sqrt{N^{B_k}}}\mathscr{L}^{-1}\left(\frac{\lambda^{iB_k}}{\sqrt{N^{B_k}}}\right). \tag{A.6}$$

References

Arruda, E.M., Boyce, M.C., 1993. A three-dimensional constitutive model for the large stretch behavior of rubber elastic materials. J. Mech. Phys. Solids 41, 389–412.

Bažant, P.J., Oh, B.H., 1986. Efficient numerical integration on the surface of a sphere. Z. Angew. Math. Mech. 66, 37–49.

Beatty, M.F., Krishnaswamy, S., 2000. A theory of stress-softening in compressible isotropic materials. J. Mech. Phys. Solids 48, 931–965.

Bergström, J.S., Boyce, M.C., 1998. Constitutive modeling of the large strain time-dependent behavior of elastomers. J. Mech. Phys. Solids 46, 931–954.

Boyce, M.C., Arruda, E.M., 2000. Constitutive models for rubber elasticity: a review. Rubber Chem. Technol. 73, 504–523.

Diani, J., Gilormini, P., in press. Combining the logarithmic strain and the full-network model for a better understanding of the hyperelastic behavior of rubber-like materials. J. Mech. Phys. Solids.

Diani, J., Brieu, M., Vacherand, J.M., Rezgui, A., 2004. Directional model for isotropic and anisotropic rubber-like materials. Mech. Mater. 36, 313–321.

Dorfmann, A., Ogden, R.W., 2004. A constitutive model for the Mullins effect with permanent set in particle-reinforced rubber. Int. J. Solids Struct. 41, 1855–1878.

Gentot, L., Brieu, M., Mesmacque, G., 2004. Modeling of stress-softening for elastomeric material. Rubber Chem. Technol. 77, 758–769.

Govindjee, S., Simo, J., 1991. A micro-mechanically based continuum damage model for carbon black-filled rubbers incorporating Mullins' effect. J. Mech. Phys. Solids 39, 87–112.

Hart-Smith, L.J., 1966. Elasticity parameters for finite deformations of rubber-like materials. J. Appl. Math. Phys. 17, 608–625.

Harwood, J.A.C., Payne, A.R., 1966. Stress softening in natural rubber vulcanizates III. Carbon black filled vulcanizates. J. Appl. Polym. Sci. 10, 315–323.

Holzapfel, G.A., Gasser, C.T., 2001. A viscoelastic model for fiber-reinforced composites at finite strains: continuum basis, computational aspects and applications. Comput. Methods Appl. Mech. Eng. 190, 4379–4403.

Holzapfel, G.A., Simo, J., 1996. A new viscoelastic constitutive model for continuous media at finite thermomechanical changes. Int. J. Solids Struct. 33, 3019–3034.

Horgan, C.O., Ogden, R.W., Saccomandi, G., 2004. A theory of stress softening of elastomers based on finite chain extensibility. Proc. Roy. Soc. Lond. A 460, 1737–1754.

Huber, N., Tsakmakis, C., 2000. Finite deformation viscoelasticity laws. Mech. Mater. 32, 1–18.

Itskov, M., Aksel, N., 2004. A class of orthotropic and transversely isotropic hyperelastic constitutive models based on a polyconvex strain energy function. Int. J. Solids Struct. 41, 3833–3848.

Kaliske, M., Nasdala, L., Rothert, H., 2001. On damage modelling for elastic and viscoelastic materials at large strain. Comput. Struct. 79, 2133–2141.

Laiarinandrasana, L., Piques, R., Robisson, A., 2003. Visco-hyperelastic model with internal state variable coupled with discontinuous damage concept under total Lagrangian formulation. Int. J. Plast. 19, 977–1000.

Lambert-Diani, J., Rey, C., 1999. New phenomenological behavior laws for rubbers and thermoplastic elastomers. Eur. J. Mech. A/Solids 18, 1027–1043.

Le Tallec, P., Rahier, C., Kaiss, A., 1993. Three-dimensional incompressible viscoelasticity in large strains: formulation and numerical approximation. Comput. Methods Appl. Mech. Eng. 109, 233–258.

Lion, A., 1998. Thixotropic behaviour of rubber under dynamic loading histories: experiments and theory. J. Mech. Phys. Solids 46, 895–930.

Marckmann, G., Verron, E., Gornet, L., Chagnon, G., Charrier, P., Fort, P., 2002. A theory of network alteration for the Mullins effect. J. Mech. Phys. Solids 50, 2011–2028.

Miehe, C., 1995. Discontinuous and continuous damage evolution in Ogden-type large-strain elastic materials. Eur. J. Mech. A/Solids 14, 697–720.

Miehe, C., Keck, J., 2000. Superimposed finite elastic–viscoelastic–plastoelastic stress response with damage in filled rubbery polymers. Experiments, modelling and algorithmic implementation. J. Mech. Phys. Solids 48, 323–365.

Mullins, L., 1948. Effect of stretching on the properties of rubber. J. Rubber Res. 16, 275–289.

Mullins, L., 1969. Softening of rubber by deformation. Rubber Chem. Technol. 42, 339–362.

Mullins, L., Tobin, N.R., 1947. Theoretical model for the elastic behavior of filler-reinforced vulcanized rubbers. Rubber Chem. Technol. 30, 551–571.

Ogden, R.W., 1972. Large deformation isotropic elasticity on the correlation of theory and experiment for incompressible rubber-like solids. Proc. Roy. Soc. Lond. A 326, 565–584.

Ogden, R.W., Roxburgh, D.G., 1999. A pseudo-elastic model for the Mullins effect in filled-rubber. Proc. Roy. Soc. Lond. A 455, 2861–2877.

Pawelski, H., 2001. Softening behavior of elastomeric media after loading in changing directions. In: Besdo, D., Schuster, R.H., Ihlemann, J. (Eds.), Proceedings of the Second European Conference on Constitutive Models for Rubber, Balkema, pp. 27–34.

Reese, S., 2003. A micromechanically motivated material model for the thermo-viscoelastic material behaviour of rubber-like polymers. Int. J. Plast. 19, 909–940.

Reese, S., Govindjee, S., 1998. A theory of finite viscoelasticity and numerical aspects. Int. J. Solids Struct. 35, 3455–3482.

Rivlin, R.S., Saunders, D.W., 1951. Large elastic deformations of isotropic materials. Experiments on the deformation of rubber. Philos. Trans. Roy. Soc. A 243, 251–288.

Sidoroff, F., 1974. Un modèle viscoélastique non linéaire avec configuration intermédiaire. J. Mécanique 13, 679–713.

Simo, J.C., 1987. On a fully three-dimensional finite-strain viscoelastic damage model: formulation and computational aspects. Comput. Methods Appl. Mech. Eng. 60, 153–173.

Treloar, L.R.G., 1975. Physics of Rubber Elasticity, third ed. University Press, Oxford.